Engineering Materials

Anand Krishnan
Anil Chuturgoon *Editors*

Integrative Nanomedicine for New Therapies

Springer

Engineering Materials

This series provides topical information on innovative, structural and functional materials and composites with applications in optical, electrical, mechanical, civil, aeronautical, medical, bio- and nano-engineering. The individual volumes are complete, comprehensive monographs covering the structure, properties, manufacturing process and applications of these materials. This multidisciplinary series is devoted to professionals, students and all those interested in the latest developments in the Materials Science field.

More information about this series at http://www.springer.com/series/4288

Anand Krishnan · Anil Chuturgoon
Editors

Integrative Nanomedicine for New Therapies

Springer

Editors
Anand Krishnan
Department of Chemical Pathology
School of Pathology
Faculty of Health Sciences
and National Health Laboratory Service
University of the Free State
Bloemfontein, South Africa

Anil Chuturgoon
School of Laboratory Medicine
and Medical Sciences
University of KwaZulu-Natal
Durban, South Africa

ISSN 1612-1317 ISSN 1868-1212 (electronic)
Engineering Materials
ISBN 978-3-030-36259-1 ISBN 978-3-030-36260-7 (eBook)
https://doi.org/10.1007/978-3-030-36260-7

This Springer imprint is published by the registered company Springer Nature Switzerland AG
The registered company address is: Gewerbestrasse 11, 6330 Cham, Switzerland

Preface

Nanotechnology is gaining popularity in modern medicine and helping to improve our quality of life. The rapidly changing pace of life necessitates rapid progress in scientific and medical research to ensure the individuals' good health and well-being. The nanotechnology "tsunami" offers novel insights into diseases and several life-threatening illnesses. These insights include rapid diagnosis and therapy of diseases such as cancer and infectious diseases. This book integrates the science of nanotechnology and medicine and its applications in nanomedicine. The information is intended for a wide audience researching in science and medicine.

The work covers basic techniques in the synthesis of nanomaterials, their biohazards, applications in diseases, drug delivery systems and their novel aspects as nutraceuticals. Taken together, the information provides the state-of-the-art solutions previously difficult to treat diseases, with limited adverse health outcomes due to therapy.

This book appeals to researchers in chemistry, physics, biochemistry, drug discovery, nutrition and medicine interested in cutting-edge research with relevance to progress in contemporary biomedicine. Some specific disease applications are included and covered extensively by including the latest innovative and relevant information of nanomedicine.

All the chapters of this book were prepared by expert researchers who have made substantial contributions to the fields of nanotechnology, drug design and delivery and nanomedicine. Each chapter is presented well and contains illustrations that will captivate the reader's interest.

We believe that that this book will substantially increase our knowledge on and applications of nanotechnology in medicine to help curb the exponential increase in human diseases.

Bloemfontein, South Africa — Anand Krishnan
Durban, South Africa — Anil Chuturgoon

The original version of this book was revised: Book Editor affiliation updated and co-author's name has been corrected in the Chapter "Nanomedicines in Tuberculosis: Diagnosis, Therapy and Nanodrug Delivery". The correction to this book can be found at https://doi.org/10.1007/978-3-030-36260-7_15

Contents

About the Editors

Dr. Anand Krishnan, D.Tech., PrchemSA has expertise in organic chemistry/medical biochemistry/integrative medicine/nano(bio)technology/drug discovery. He received his doctoral degree in organic chemistry in the Department of Chemistry, Durban University of Technology, in collaboration with the Department of Medical Biochemistry, University of KwaZulu-Natal, in 2014. He completed his master's degree in organic chemistry from Bharathiar University, India, and bachelor's degree in chemistry from Madurai Kamaraj University, India. He was Postdoctoral Researcher at Durban University of Technology, South Africa, from November 2014 to November 2016. He has published many scientific articles in international peer-reviewed journals and has authored many chapters as well as review articles. He was recognised for his contributions and received awards from national and international organisations. He has been awarded Best Postdoctoral Researcher Award for 2016 and 2017 from Durban University of Technology and Young Scientist Researcher Award 2016 from Pearl Foundation. He is Member of various editorial boards of the journals of the international reputation. His research interests include organic synthesis, catalysis, heterocyclic chemistry, cannabis chemistry, drug discovery, phytonanotherapy, extracellular vesicles, nanotoxicology and chemical pathology.

Currently, he received prestigious Innovation Post-doctoral Research Fellowship from National Research Foundation (NRF), South Africa and conducting research at the Department of Chemical Pathology, School of Pathology, Faculty of Health Sciences and National Health Laboratory Service (NHLS), University of the Free State, Bloemfontein, South Africa.

Prof. Anil Chuturgoon, Ph.D. is Head of Discipline of Medical Biochemistry in the School of Laboratory Medicine and Medical Sciences at the University of KwaZulu-Natal (UKZN), Durban, South Africa. He completed his B.Sc., B.Sc. (Hons) and M.Sc. degrees at the University of Natal. He thereafter obtained his doctoral degree in toxicology and epigenetics from UKZN. He is passionate about research and shaping young minds to think critically. He is Member of several scientific associations and editorial boards. He received the Distinguished Teacher Award for excellence in teaching. He is NRF-rated Scientist and was placed in the top 30 UKZN researchers for 2016, 2017 and 2018. He has successfully supervised over 50 masters' and 27 doctoral students. He has over 110 refereed publications, 12 chapters in books and over 200 conference proceedings.

Basic Techniques to Investigate the Nanostructured Materials

Navaneethan Duraisamy, Kavitha Kandiah and Balagurunathan Ramasamy

Abstract This chapter is to deliver the basic methods for the characterizations of nanostructured materials. There are different shapes of materials existing in the nanomaterials such as particles, sheets, roads, dots, balls and films. The crystalline structures and surface morphology of nanomaterials are clearly calibrated using advanced techniques such as X-ray diffraction, Field emission scanning electron microscopy and transmission electron microscopy. The chemical compositions and purity of materials are examined by Energy dispersive X-ray analysis, Fourier transform infrared analysis and X-ray photoelectron spectroscopy. The biological studies of nanomaterials are examined using bioactivity, anti-microbial activity and bio degradability. This review gives a comprehensive understanding of the physico-chemical and biological nature of the nanomaterials.

1 Introduction

NANO is the heart core research field in the emerging technology; utilize nanomaterials in the range of 1–100 nm sizes with different shapes. The size of the materials and shapes are having a potential for various applications in biomedical, energy harvesting, energy storage, fertilizers and agriculture. The tuning of sizes and shapes are more important to adopting the materials for targeting application. Designing the specific structure of nanomaterials would be investigated using various advanced technical tool in the field of material science and technology (Wu et al. 2018; Murty et al. 2012; Duraisamy et al. 2013, 2018). But, it is not applicable to use same technical tools for all types of samples (conducting polymers, metal oxides, metal

Navaneethan Duraisamy and Kavitha Kandiah are equally contributed.

N. Duraisamy (✉)
Department of Chemistry, J.K.K. Nataraja College of Arts and Science, Komarapalayam, Namakkal, Tamil Nadu, India

K. Kandiah · B. Ramasamy (✉)
Department of Microbiology, Periyar University, Salem, Tamil Nadu, India
e-mail: rbalaguru@periyaruniversity.ac.in

A. Krishnan and A. Chuturgoon (eds.), *Integrative Nanomedicine for New Therapies*, Engineering Materials,
https://doi.org/10.1007/978-3-030-36260-7_1

sulphides, carbon materials, biomolecules and etc.) due to the influence of materials handling and sensitivity. The selection of tools is mainly depend on the materials nature, for example, Kirk et al. reported that the surface structure of biological sample can be examined using environmental scanning electron microscopy (ESEM) but not in normal scanning electron microscopy (SEM) because it is more important to maintain the nature (alive) of biological sample. However, other than biological samples, normal SEM technique is more preferable to determine the shapes, sizes and surface of materials (ref-my paper). In order to analysis the biological sample at high resolution (in depth view) under freezing condition, Cryo-SEM is more feasible than ESEM but expensive (Kirk et al. 2009).

In this chapter, we have focused on the basic technical tools for the investigation of nanomaterials such as X-ray diffraction (XRD), Fourier transform infrared spectrometer (FT-IR), Raman spectroscopy, Dynamic Light Scattering, Brunauer–Emmett–Teller surface area analysis and mechanical characterization, Scanning electron microscopy, Transmission electron microscopy (TEM) and nano indentation. The above tools are significantly play an vital role to analysis the structural crystallinity, crystalline size, phase nature, presence of functional groups, surface purity, surface area, shapes, sizes, presence of defects and mechanical strength of the materials. This chapter is providing strong background to understand the basic tools for the investigation of nanomaterials, where strongly support to bring out the anticipated materials in the field of science and technology.

2 X-Ray Diffraction Analysis

The crystallographic nature of prepared samples was evaluated by X-ray diffraction (XRD) analysis. The XRD patterns were used for structural determination of the prepared samples. The structural crystallinity of TiO_2 nanoparticle (pure) and its composites were examined by XRD spectrometer (X'Pert PRO; PANalytical, the Netherlands) with a radiation source of CuK_α ($\lambda = 1.5406$ Å) at 30 mA current with an accelerating voltage of 40 kV. The synthesized samples were scanned at 2θ (angle) and a range of 10–80° with an increment of 0.05°. The diffraction patterns of the synthesized samples were confirmed with help of standard reference data, that is, Joint Committee on Powder Diffraction Standards (JCPDS). The average crystallite size was determined using Scherrer formula (Choi et al. 2004; Kavitha et al. 2013a):

$$D = \frac{k\,\lambda}{\beta \cos\theta} \tag{2.1}$$

where D is the crystal size, k—Scherrer constant, λ—wavelength (1.5406 Å), β—full width at half maximum and θ—diffraction angle.

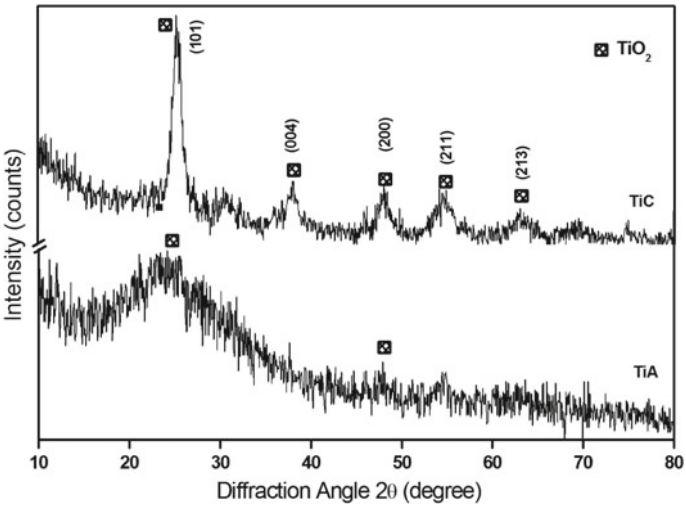

Fig. 1 X-ray diffraction patterns of prepared TiO_2 nanosamples

2.1 Metal and Metal Oxide

The crystalline nature of the TiO_2 nanoparticles at 393 K (TiA) and 673 K (TiC) is analysed by X-ray diffraction (XRD) analysis, as shown in Fig. 1. It is ascertained that TiA is amorphous in nature, which is in line with the results of previous studies (Yin et al. 2001). The high-intensity peak seen in TiC at 25.328° (2θ) is in accordance with the characteristic diffraction peak of TiO_2 anatase phase (JCPDS file no. 21-1272). The peak intensity and sharpness of TiC show that sintered samples do not have any impurities. The crystallite size of the TiO_2 nanosample is determined by Scherrer equation (Choi et al. 2004; Kavitha et al. 2013a). Owing to the amorphous nature of TiA, no peak is observed to calculate the crystallite size, whereas TiC shows 8 nm crystallite sizes.

2.2 Carbon and Polymer Materials

The XRD pattern of graphite, graphene oxide (GO), graphene (rGO) and polymer is shown in Fig. 2. The high-intensity peak appearing at 10–12.4 (2θ) is in accordance with the characteristic diffraction peak of graphene oxide and peak at 24.7–26.6° is for reduced graphene oxide and graphite, (JCPDS no. 89-7213). In addition, the peak intensity and peak sharpness shows that the samples do not have significant impurities. According to the Scherrer formula and 2θ angle, the average crystallite size of the extracellular reduced graphene oxide is calculated as 5 nm and GO is 7 nm (Kavitha et al. 2013b).

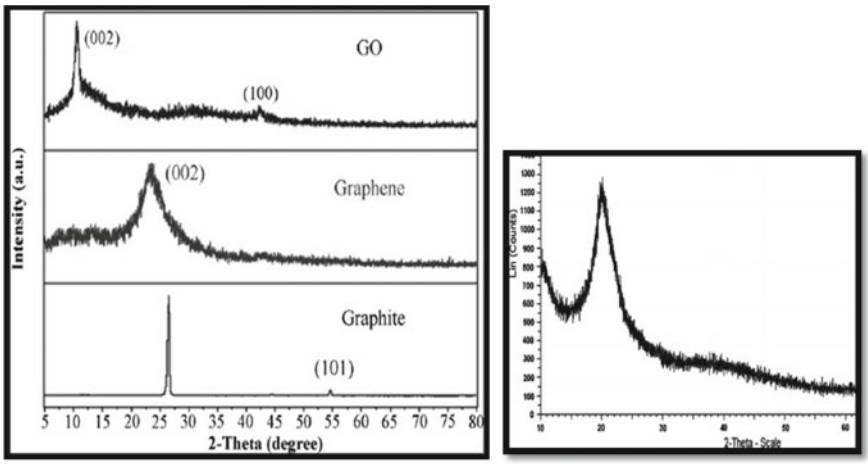

Fig. 2 X-ray diffraction patterns carbon and polymer nanosamples

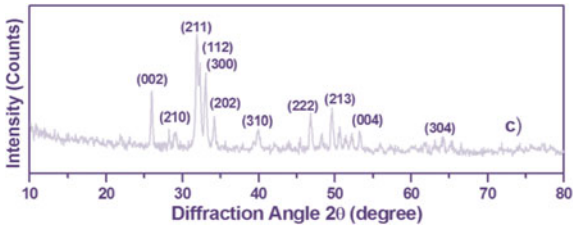

Fig. 3 XRD analysis of pure HAp obtained at 150 °C

2.3 Ceramic Materials

Figures 3 shows the XRD pattern of HAp treated at 150 °C for time period of 15 h at 150 °C.

All the peaks of d spacing are identified and matched well with a standard JCPDS file (09-0432). The XRD patterns confirmed the high crystalline nature of HAp, where identified on the basis of intensity and peak width. No other crystalline phase is present besides HAp. The crystallite size is calculated from Scherrer's formula. The crystallite size was 26.9232 nm. The crystallinity of HAp increased with an increasing the reaction temperature and time (Rajkumar et al. 2011).

2.4 Polymers and Composites

Figure 4 illustrated the XRD pattern of temperature-variant composite samples. The obtained broad diffraction patterns (25.32° and 26.6°) were confirmed the formation

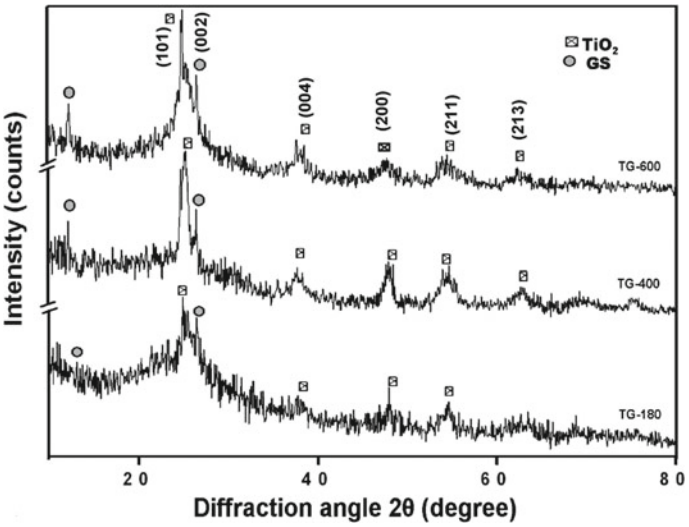

Fig. 4 XRD analysis of titania–graphene composite

of crystalline titania-graphene oxide composite (JCPDS file no. 21-1276) (Zhang et al. 2010; Krishnamoorthy et al. 2013).

However, a small hump at 12.7° was clearly identified with increasing the sintering temperature of titania-graphene oxide nanocomposite, which was due to trace amount of graphite oxide (Krishnamoorthy et al. 2013). The average crystallite size was 3.01, 3.13, 3.23 nm respectively for 180, 400 and 600 °C. As similar with previous studies, this study also conforms the addition of carbon into the titania reduces the crystallite size (Manivasakan et al. 2010; Krishnamoorthy et al. 2013). Moreover, this study disclosed that the crystallite size increased with increasing sintering temperature of composite materials, which was due to effect of temperature during the nucleation process (Manivasakan et al. 2010).

3 Dynamic Light Scattering

The particle size distribution was calculated via particle size analyser (Nanophox; Sympatec, Clausthal-Zellerfeld, Germany). This was simply working on the principle of dynamic light scattering with three-dimensional photon cross-correlation method. Here, light source was He–Ne laser with a maximum intensity of 10 mW (λ = 632.8 nm).

A stable colloidal solution was obtained by dispersing the nanoparticles in an aqueous solution using a sonochemical reactor (Vibra-Cell; Sonics, USA). The solution of dispersed nanoparticles was taken into the liquid cell and measured from 1 to1000 nm at 90° (scattering angle).

The particle size distribution (PSD) measured for both samples TiA and TiC was illustrated in Fig. 5a, b, confirming that the PSD of synthesised samples is below 50 nm. However, the PSD of TiA (25–50 nm) is wider than that of the TiC (16–28 nm) (Kavitha et al. 2013a, c). This reduction is due to the uniform arrangement of

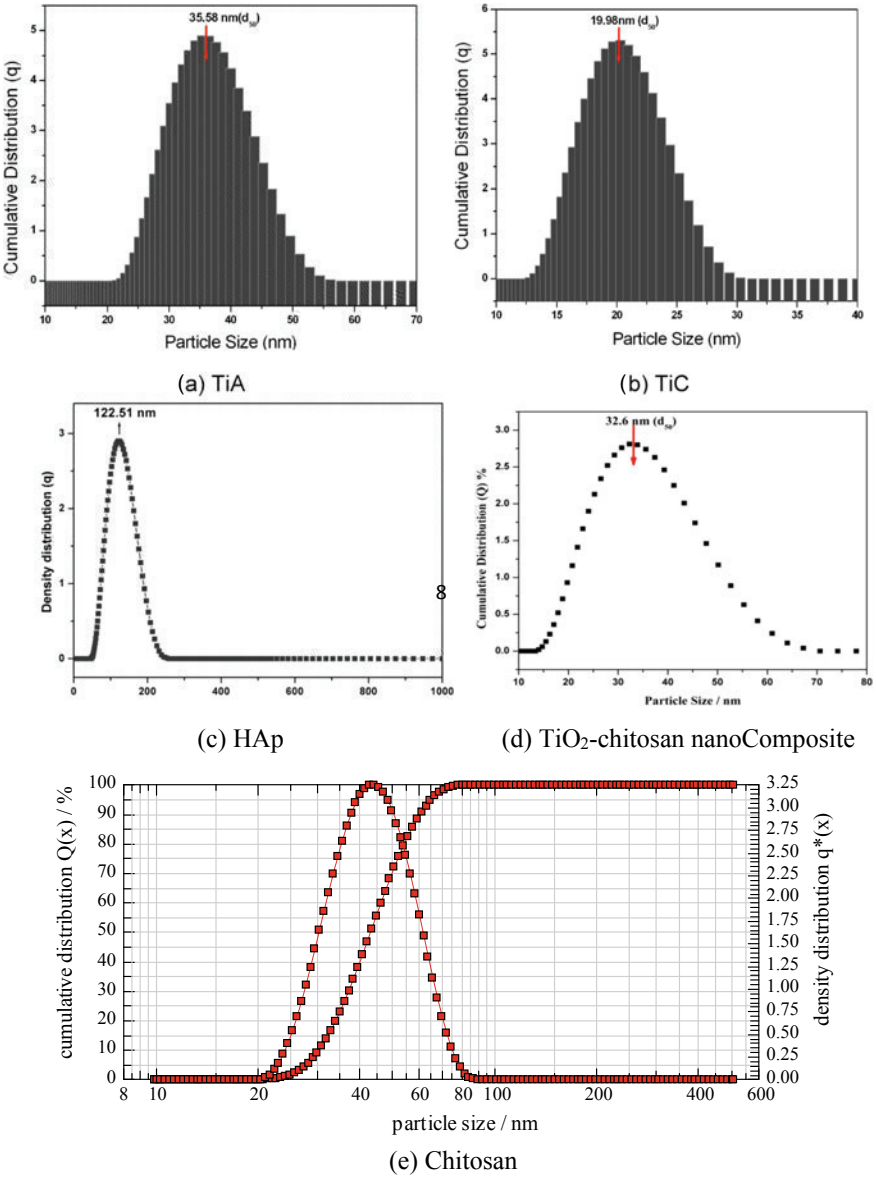

Fig. 5 Particle size distribution of nano-TiO_2, HAp, nanocomposite and polymer

lattice and complete removal of unnecessary components present in the sample during sintering (Manivasakan et al. 2010). Figure 5c illustrates the particle size distribution of the HAp obtained at 423 K for 15 h using a laser particle size analyzer. The mean particle size distribution of HAp is 122.51 nm (Rajkumar et al. 2011). Figure 5d shows the 15–65 nm of particle size distribution of TiO_2-chitosan nanocomposite material (Kavitha et al. 2013a, c). Figure 5e shows the PSD of chitosan is obtained from 20 to 80 nm.

4 Fourier Transform Infrared Spectroscopy

Fourier transform infrared spectrometer (FTIR; Spectrum 100; PerkinElmer, USA) was used to identify the functional group of prepared samples based on the atomic vibrations of a molecule. The peaks appearing in the absorption spectrum correspond to the frequency of the samples. The functional groups and chemical bonds in pure TiO_2 nanoparticles and their composites were analysed using FTIR spectroscopic studies. For FT-IR study, a small pellet was prepared via simple mixing of examine sample with known materials of potassium bromide in the ratio of 2:200 (w/w), which was pressed under hydraulic pressure pellet maker (pressing weight was 125 kg cm^{-2}). The absorption spectra analyses were carried out on the pellets at a λ range of 4000–400 cm^{-1} with 1 cm^{-1} resolution.

4.1 Metal Oxide and Ceramics

The functional groups of the prepared TiO_2 nanoparticles are listed in Fig. 6a shows that the broad peaks obtained at 400–900 cm^{-1}correspond to the characteristic peak of Ti–O–Ti stretching mode (Kavitha et al. 2013a, b). While sintering the TiO_2, the

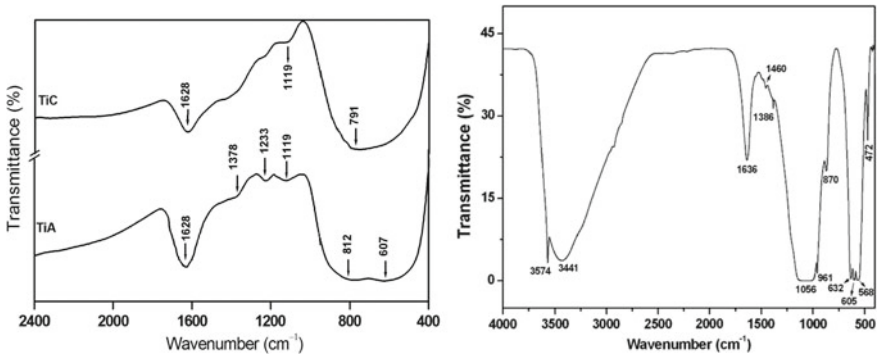

Fig. 6 FTIR analysis of TiO_2 nanosamples

broad Ti–O–Ti covalent band is narrowed down to 550–800 cm^{-1} due to transformation of Ti (OH) into TiO_2. The vibration bands obtained at 1119 and 1233 cm^{-1} were assigned, respectively, to the stretching and bending modes of Ti–O–C, and Ti–OH surface groups (Manivasakan et al. 2010, Al-Sagheer and Merchant 2011, Zawadzki and Kaczmarek 2010). The Ti–OH group accelerates the formation of apatite nucleation due to the release of Ca^{2+}, Na^{+} or K^{+} ions (Nakayama and Hayashi 2007). The CH_3 stretching is observed near 1380 cm^{-1}. The presence of carbon band in TiO_2 was the influence of inadequate evaporation of solvents during the synthesis. In addition, the peak observed at 1628 cm^{-1} was responsible for hydroxyl group, which is gradually reduced while sintering the sample TiA into TiC.

FTIR has been employed to analyse the characteristic bands of the prepared samples. The FTIR spectra of the HAp are prepared by hydrothermal treatment at 423 K for 15 h as shown in Fig. 6b. The characteristic bands of the PO_4^{3-} groups are observed at 472, 568, 605, 961 and 1056 cm^{-1} (Rajkumar et al. 2011, 2013). The peaks observed at 632 cm^{-1} are due to O–H bending deformation mode. The stretching vibration of lattice OH^{-} ions is attributed at 3574 cm^{-1}. The peaks at 1460, 1386 and 870 cm^{-1} are due to atmospheric carbon dioxide (Chen et al. 2007; Zhao et al. 2009). The bands registered at 3441 and 1636 cm^{-1} were ascribed to adsorb H_2O (Kavitha et al. 2013c, Vallet-Regi 2001). Based on the FTIR result, it can be concluded that there is no obvious peak for any other impurity.

4.2 Carbon and Composite Materials

FTIR analysis of GO and rGO (Fig. 7a) shows, the presence of C–OH, C–O and C–O–C peaks in GO nanosheets but, not prepared rGO. Instead of oxygen and hydroxyl groups, rGO has C–C band, which confirms the occurrence of reduction process. FTIR is clearly shows and validate that, the reduction of multiple thick GO layers to thin rGO layer in nano dimension (Kavitha et al. 2013b, d; Krishnamorrthy et al.

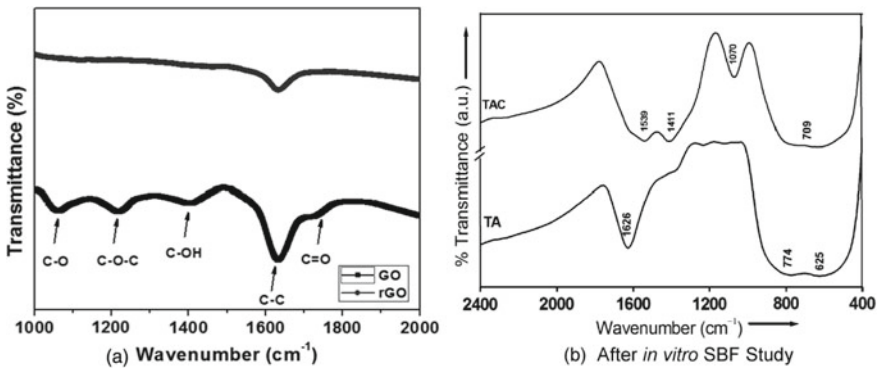

Fig. 7 Fourier transform infrared spectroscopy of graphene sample

2013). Similarly, Fig. 7b shows the HAp formation on nano-TiO_2 and nano-TiO_2–chitosan coated Ti-6Al-4 V. In addition, the presence of functional groups such as Ti–O–Ti (400–800 cm^{-1}), Ti–OH (1106), Ti–O–C (1233 cm^{-1}), and C–O (1392 cm^{-1}) and CO_3^{2-} (1415 cm^{-1}) peak after bioactivity were also confirm the formation of HAp. This result supported the TAC coating on Ti-6Al-4 V, helps in the enhancement of cell growth for tissue engineering applications.

5 Microscopic and Spectroscopic Analyses

Transmission electron microscopy (TEM) working at 120 kV a beam of electron is transmitted through the specimen. An image was generated by the interaction of the electrons transmitted via sample. Further, the image was enlarged and followed by clear focus on a fluorescent display or a layer of photographic film. The morphology and particle size of the pure TiO_2 nanoparticle and its composites were examined by analysing the image obtained from TEM (CM 200; Philips, USA). Well-dispersed material was loaded on TEM grid and followed by drying with a help of IR lamp for ~30 min. The images of the samples were then captured from dried grids. The image of TEM exhibited a zooming up to 1,000,000 × with a good resolution than 10 Å. A particle size was measured from the randomly selected areas of each sample, and then, the average size was calculated. In addition, selected area electron diffraction (SAED) pattern of the samples was obtained. The obtained images showed the crystalline nature and lattice arrangements of the prepared samples.

In SEM, a high-energy electron beam with 25 keV (accelerating voltage) was used to investigate the materials surface (morphology, shape and size). In addition, an elemental analysis of the material was also evaluated using energy-dispersive X-ray coupled with SEM (SEM–EDX; JSM 6390; JEOL, Japan). For the SEM–EDX analysis, preparation of samples was carried out by smearing 1 μg sample on the carbon tape (conductive and adhesive nature) mounted on a brass stub and then, the samples were gold or platinum coated (thickness around 5–10 nm achieved within ~60 s) via applying a current of 20 mA using a magnetron sputtering. The deposition of calcium (Ca) and phosphate (P) on the surface of the 1.5 SBF-incubated samples was quantified before and after the bioactivity study using X-ray fluorescence spectrometry (XRF; EDX-720; Shimadzu, Japan).

A FE-SEM image, the particles reveals spherical like TiO_2 (Fig. 8a), nanorod like HAp (Fig. 8b), leaf like GO (Fig. 8c) and leaf and spherical mixed morphology of Nanocomposites (Fig. 8d) (Kavitha et al. 2013d; Rajkumar et al. 2011). In addition, the EDX of all the prepared nano-samples shows the purity and exact material preparation. There is no contamination was found in EDX of all the nano-samples (Fig. 8).

The primary particle sizes of the prepared nanosample are shown in Fig. 9. TEM images confers the exact size of each defined crystallite existed in the particles. In addition, all the prepared particles are diffracted at 50 nm range and the average

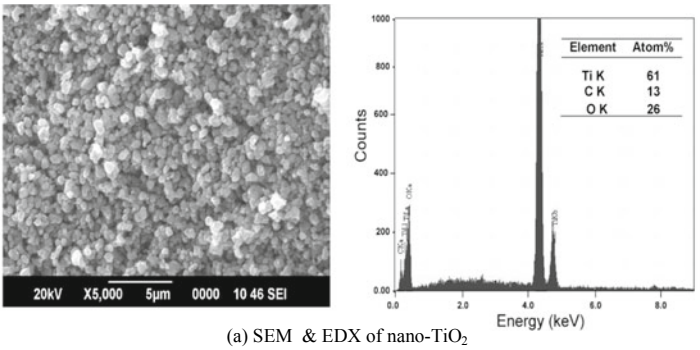

(a) SEM & EDX of nano-TiO_2

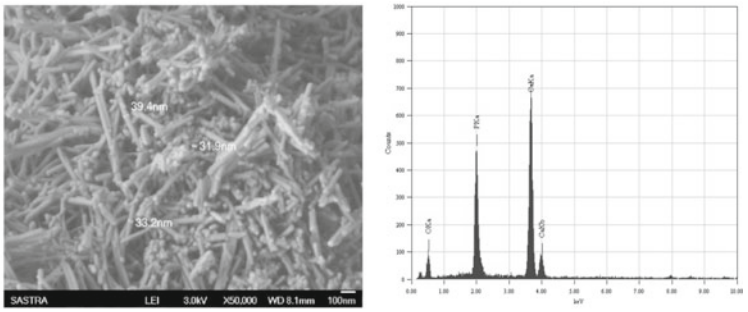

(b) SEM & EDX of nano-HAp

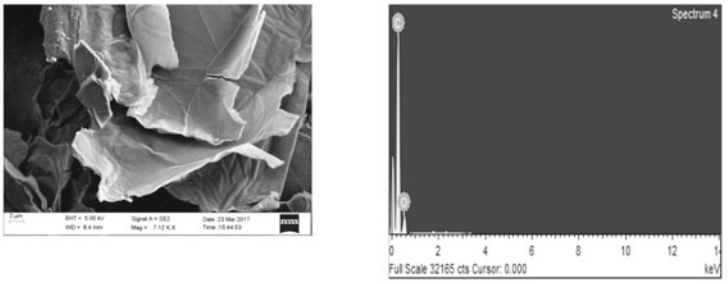

(c) SEM & EDX of nano-Graphene oxide (GO)

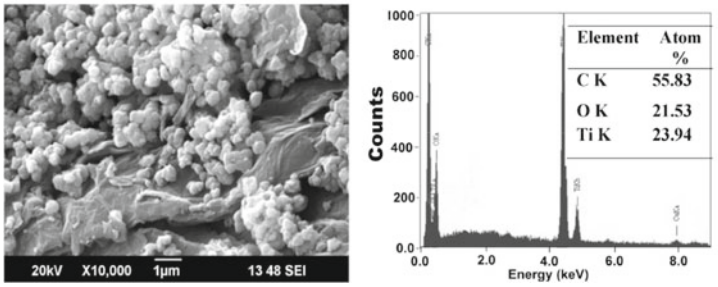

(d) SEM & EDX of TiO_2-Graphene nanocomposite

Fig. 8 SEM and EDX of nanosamples

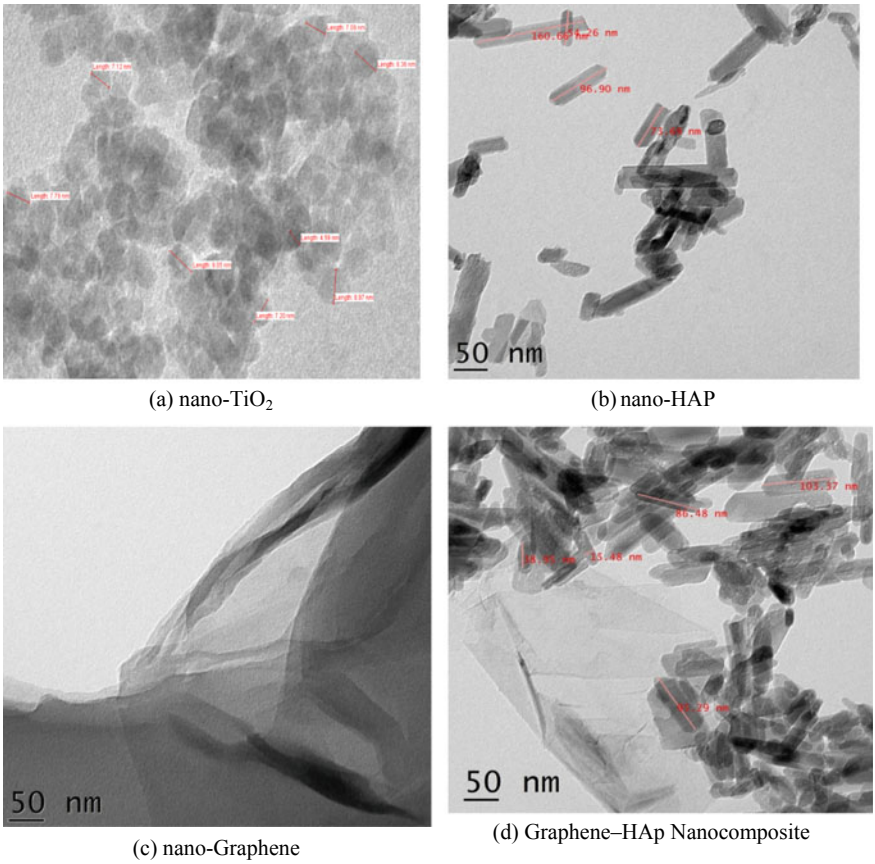

(a) nano-TiO_2 (b) nano-HAP

(c) nano-Graphene (d) Graphene–HAp Nanocomposite

Fig. 9 TEM images of prepared nanosamples

mean particle size is noted. The particle size of TiO_2, HAp and composite is respectively as 3.5 nm, 8.19 nm and 8.86 nm. Moreover, the sintering temperature, rotation speed, pH, precursor material and synthesis procedure were a vital role to determine the particle size and agglomeration of the finer particles (Manivasakan et al. 2010, Kavitha et al. 2013d, Rajkumar et al. 2011; Xu et al. 2006).

6 Brunauer–Emmett–Teller Surface Area Analysis

The specific surface area (SSA) of the samples was calculated with respect to the Brunauer–Emmett–Teller (BET) method (Barrett et al. 1951) using BET Surface Area Analyser (Autosorb AS-1MP; Quantachrome, USA). A well-known isotherm equation for multilayer adsorption was proposed by Brunauer, Emmett and Teller

in 1938. Gas sorption (both adsorption and desorption) at the surface of dry solid powder was commonly used to determine the surface area of the nanomaterials. In this method, the nanoparticles were first heated and degassed under vacuum for 3 h to eliminate the physisorbed moisture. The degassing temperature of the samples depends on the melting and decomposition nature of its own. The physisorption analysis was carried out with N_2 adsorption–desorption measurements under liquid-nitrogen temperature (77 K). A very low working temperature was used to avoid unnecessary thermal damage on the materials surface. Different quantities of gas molecules were adsorbed and desorbed at various amounts of gas. The pore structure (distribution of pore size and its micro/mesopore volume) of the prepared samples was performed by Barrett–Joyner–Halanda method using BET Surface Area Analyser (Manivasakan and Rajendran 2011).

The obtained SSA of the prepared nanocomposites shows TiO_2-graphene at different temperature. In addition, the increase of SSA with respect to higher sintering temperature is shown in Fig. 10 (Kavitha et al. 2013d). The full isotherms of the prepared Nanocomposites at different ratio of TiO_2-graphene: TG.25, TG.5, TG1, TG2, and TG4 samples were found to be 167.98, 186.52, 212.85, 216.04, and 234.56 (Fig. 11) Kavitha et al. 2013b). SSA, total pore volume, and pore diameters were increased with increasing graphene content in the composites. However, the surface area and total pore volume of TGS nanocomposites were initially reduced up to 0.5 g (wt%) of graphene (TG.5), which was due to the total occupation of TiO_2 with low graphene content (Kavitha et al. 2013b). In addition, higher content of TiO_2 tend to collapse the basal spacing of graphene sheet, where confirmed by SEM (Fig. 4) and TEM (Fig. 5). This result was clearly confirmed that TG1, TG2, and TG4 samples exhibited optimal ratio for the improved interactions with the bone-inducing cells. The large surface area and pore size of TG1–TG4 possess three dimensional way of cell growth with healthier cells and nutrients attachment from the body as defined as earlier (Kavitha et al. 2013b, Zhang et al. 2010, 2012, Akhavan et al. 2010).

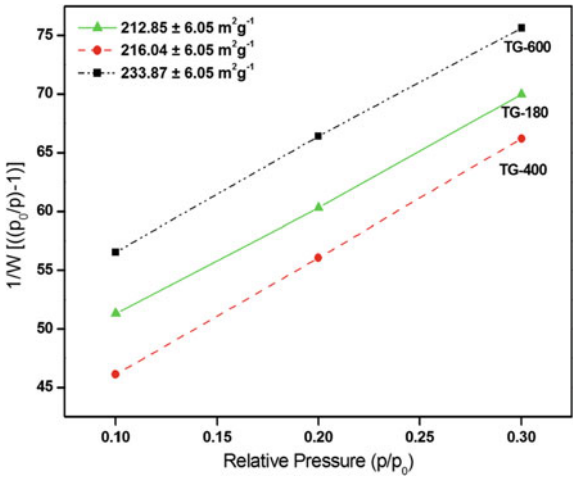

Fig. 10 BET surface area analysis of titania–graphene composites

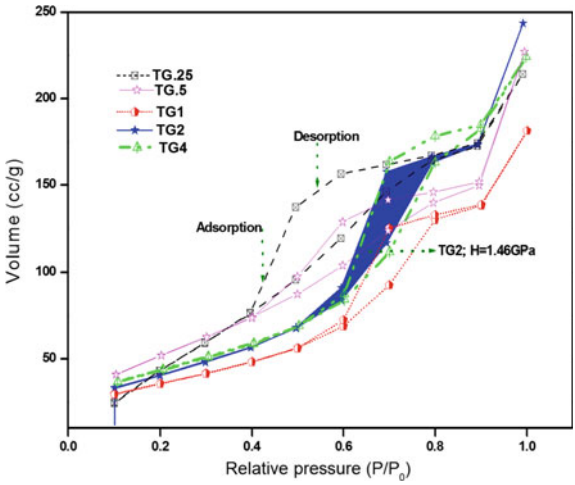

Fig. 11 BET full isotherm of the cure of titania–graphene nanocomposites

7 Mechanical Characterisation

The mechanical properties such as nano-hardness (H) and Young's modulus (E), of the nanocomposites were evaluated by TriboIndenter (Quasistatic nanoindentation, TI-700; Hysitron, USA). The measured force versus displacement curve obtained from the indentation shows the mechanical properties of the materials. Indentation was carried out with a Berkovich pyramidal indenter at a constant load of 1 μN. Both loading and unloading times were keeping consent as 5 s at rate of 200 nm s^{-1} at maximum force of 1000 μN. A small volume of materials with a scan size of 10 × 10 μm was covered during the measurements. The mechanical properties of specimen were obtained using a standard relationship between the applied indentation load (P) and the measured penetration depth (h), as given below (VanLandingham et al. 2001; Yuan et al. 2008):

$$H = P_{\max}/\mathrm{A}(h_c) \tag{2.2}$$

$$E = \sqrt{\pi} \,.\, S/2\sqrt{A(h_c)} \tag{2.3}$$

where, P—applied maximum force, A(h_c)—the area of function, A—area and h_c—contact depth and S—contact stiffness from slope of the loading and unloading curves.

Mechanical testing (H and E values) of the nanocomposite is evaluated by comparison of displacement vs. force plot, using Tibo Scan V8.2 software. The measured nanohardness of pure TiO_2 (1.80 GPa) and TiO_2–chitosan (0.29 GPa) nanocomposites is shown in Fig. 12 illustrated the result of reduction in hardness and Young's

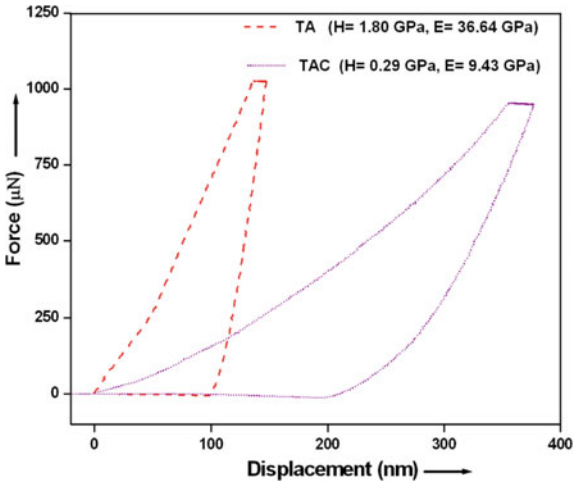

Fig. 12 Mechanical indentation results of titania–chitosan composites

moduli, while adding chitosan to TiO_2. Previous studies were support the fact of prepared composite (Kavitha et al. 2013c; Zhang et al. 2010, 2012; Akhavan et al. 2010) is hard enough to be considered a biomaterial for bone regeneration application.

8 Raman Spectra

Figure 13 illustrated the Raman analysis of TiO_2-graphene composites. The bands at 148, 396, 519 and 639 cm^{-1} were confirmed the presence of TiO_2 (Kavitha et al. 2013d). A non-destructive analysis disclosed the G and D band of graphene, where the bands observed at ~1588 and 1355 cm^{-1} along with the 2D band at 2679 cm^{-1} (Zhang et al. 2010, 2012; Akhavan and Ghaderi 2010; Selvam et al. 2013). The G and D bands intensity were increased with increasing the graphene concentration in the composites. But TiO_2 bands were reduced in composite (influence of the graphene concentration)

The slight bands shift (TiO_2 and graphene bands) towards lower wave number was detected due to the composite formation. Raman spectrum confirmed the presence graphene and the formation of TiO_2-graphene composites. Similarly, Fig. 14 shows the Raman spectra of HAp-graphene Nanocomposites. In Fig. 14, the graphene peaks such as G and D bands and HAp peak at 960–990 cm^{-1} is shown. However, in composite, the HAp peaks are suppressed by domination of graphene peaks.

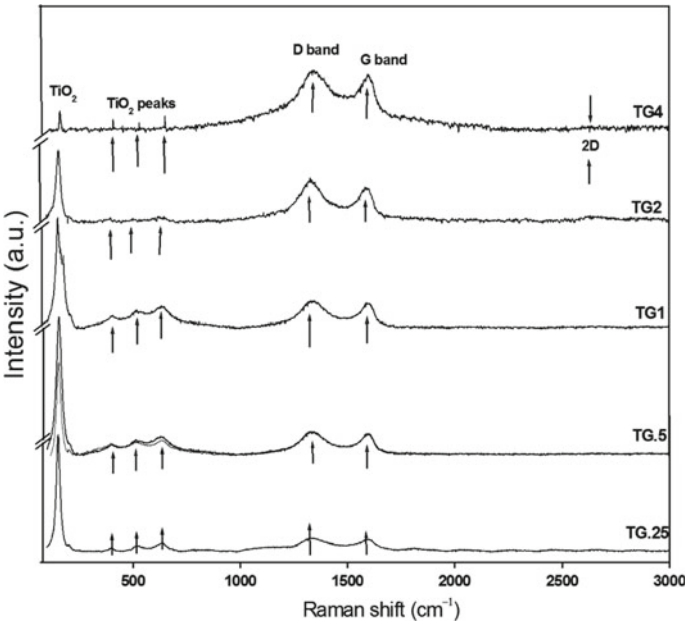

Fig. 13 Raman spectra of the TiO_2-graphene nanocomposites

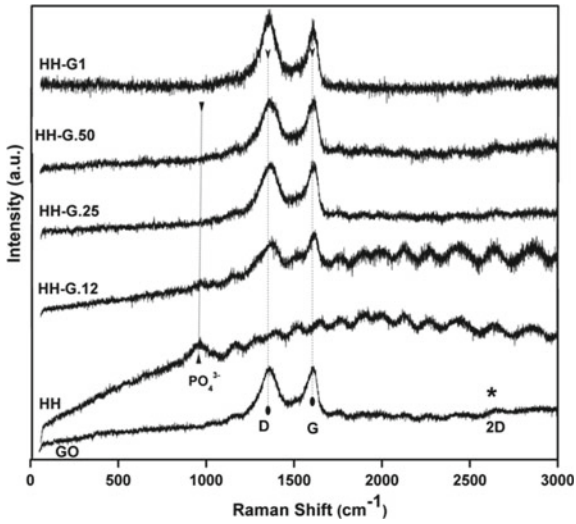

Fig. 14 Raman spectra of the HAp-graphene nanocomposites

9 Conclusion

The characterization techniques are played a significant role to investigate the physico-chemical properties of nanostructured materials. The detailed structural analysis and chemical bonding between the different molecules and surface purity were clearly explained by XRD, Raman, FT-IR analysis. The presence of elements in the synthesized materials was elucidated using EDX, XRF and XPS analysis. Here, confirmation of rGO from GO and the interaction between metal oxides and rGO were investigated. There different types of surface morphologies such as sheet structure of rGO, particles shapes of TiO_2, road like shape of Hap were clearly explained by SEM and TEM analysis. Surface to value ratio of nanomaterials (metal oxides, polymers, carbon and composites) was measured by BET. Nano-Indentation technique was used to determine the mechanical strength of materials (pure TiO_2: 1.80 GPa) and TiO_2–chitosan: 0.29 GPa) nanocomposites) for biomedical application.

Acknowledgements The author Dr. Navaneethan Duraisamy acknowledges the financial support provided by DST INSPIRE Faculty scheme (DST/INSPIRE/04/2018/001444), New Delhi. Dr. K. Kavitha acknowledges the financial support provided by Dr. D.S. Kothari Postdoctoral Fellowship (Ref. no: No. F.4–2/2006 (BSR)/BL/15–16/0225, UGC, New Delhi.

References

Akhavan, O., & Ghaderi, E. (2010). Toxicity of graphene and graphene oxide nanowalls against bacteria. *ACS Nano, 4,* 5731–5736.

Al–Sagheer, F. A., & Merchant, S. (2011). Visco–elastic properties of chitosan–titania nano–composites. *Carbohydrate Polymers, 85,* 356–362.

Barrett, E. P., Joyner, L. G., & Halenda, P. P. (1951). The determination of pore volume and area distributions in porous substances. *Journal of the American Ceramic Society, 73,* 373–380.

Chen, Y. L., Lee, H. P., Chan, H. Y., Sung, L. Y., Chen, H. C., & Hu, Y. C. (2007). Composite chondroitin-6-sulfate/dermatan sulfate/chitosan scaffolds for cartilage tissue engineering. *Biomaterials, 28,* 2294–2305.

Choi, H. C., Ahn, H. J., Jung, Y. M., Lee, M. K., Shin, H. J., Kim, S. B., et al. (2004). Characterization of the structures of size-selected TiO_2 nanoparticles using X-ray absorption spectroscopy. *Applied Spectroscopy, 58,* 598–602.

Duraisamy, N., Hong, S. J., & Choi, K. H. (2013). Deposition and characterization of silver nanowires embedded, PEDOT: PSS thin films via electrohydrodynamic atomization. *Chemical Engineering Journal, 225,* 887–894.

Duraisamy, N., Kandiah, K., Rajendran, R., Prabhu, S., Ramesh, R., & Dhanaraj, G. (2018). Electrochemical and photocatalytic investigation of nickel oxide for energy storage and wastewater treatment. *Research on Chemical Intermediates, 44,* 5653–5667.

Kavitha, K., Chunyan, W., Navaneethan, D., Rajendran, V., Valiyaveettil, S., & Vinoth, A. (2013a). In vitro gene expression and preliminary in vivo studies of temperature-dependent titania–graphene composite for bone replacement applications. *RSC Advances, 210,* 43951–43961.

Kavitha, K., Prabhu, K., Rajendran, M., Manivasankan, V., Prabu, P., & Jayakumar, T. (2013b). Optimization of nano–titania and titania–chitosan nanocomposite to enhance biocompatibility. *Current Nanoscience, 3,* 308–317.

Kavitha, K., Prabhu, M., Selvam, M., & Rajendran, V. (2013c). TiO_2–graphene nanocomposites for enhanced osteocalcin induction. *Materials Science and Engineering C, 48,* 252–262.

Kavitha, K., Sutha, S., Prabhu, M., Rajendran, V., & Jayakumar, T. (2013d). In situ synthesized novel biocompatible titania–chitosan nanocomposites with high surface area and antibacterial activity. *Carbohydrate Polymers, 93,* 731–739.

Kirk, S. E., Skepper, J. N., & Donald, A. M. (2009). Application of environmental scanning electron microscopy to determine biological surface structure. *Journal of Microscopy, 233,* 205–224.

Krishnamoorthy, K., Kim, G. S., & Kim, S. J. (2013). Graphene nanosheets: Ultrasound assisted synthesis and characterization. *Ultrasonics Sonochemistry, 20,* 644–649.

Manivasakan, P., & Rajendran, V. (2011). Synthesis of monoclinic and cubic ZrO_2 nanoparticles from zircon. *Journal of the American Ceramic Society, 94,* 410–1420.

Manivasakan, P., Rajendran, V., Rauta, P. R., Sahu, B. B., Sahu, P., Panda, B. K., et al. (2010). Effect of TiO_2 nanoparticles on properties of silica refractory. *Journal of the American Ceramic Society, 93,* 2236–2243.

Murty, B. S., Shankar, P., Raj, B., Rath, B. B., & Murday, J. (2012). Tools to characterize Nanomaterials. In: *Texbook of nanoscience and nanotechnology* (pp. 149–175). Springer. ISBN 978-3-642-28030-6.

Nakayama, N., & Hayashi, T. (2007). Preparation and characterization of poly(l-lactic acid)/TiO_2 nanoparticle nanocomposite films with high transparency and efficient photodegradability. *Polymer Degradation and Stability, 92,* 1255–1264.

Rajkumar, M., Kavitha, K., Prabhu, M., Meenakshisundaram, N., & Rajendran, V. (2013). Nanohydroxyapatite–chitosan–gelatin polyelectrolyte complex with enhanced mechanical and bioactivity. *Materials Science and Engineering C, 33,* 3237–3244.

Rajkumar, M., Meenakshi Sundaram, N., & Rajendran, V. (2011). Preparation of size controlled, stoichiometric and bioresorbable hydroxyapatite nanorod by varying initial pH, Ca/P ratio and sintering temperature. *Digest Journal of Nanomaterials and Biostructures, 6*(1), 169–179.

Selvam, M., Sakthipandi, K., Suriyaprabha, R., Saminathan, K., & Rajendran, V. (2013). Synthesis and characterisation of electrochemically–reduced graphene. *Bulletin of Material Science, 36,* 1315–1321.

Vallet-Regi, M. (2001). Ceramics for medical applications. *Journal of the Chemical Society, Dalton Transactions, 2,* 97–108.

VanLandingham, M. R., Villarrubia, J. S., Guthrie, W. F., & Meyers, G. F. (2001). Nanoindentation of polymers: An overview. *Macromolecular Symposium, 167,* 15–43.

Wu, J. B., Lin, M. L., Cong, X., Liu, H. N., & Tan, P. H. (2018). Raman spectroscopy of graphene-based materials and its applications in related devices. *Chemical Society Reviews, 47,* 1822–1873.

Xu, Q., Fan, H., Guo, Y., & Cao, Y. (2006). Preparation of titania/silica mesoporous composite with activated carbon template in supercritical carbon doixide. *Material Science and Engineering A, 435,* 158–162.

Yin, H. Y., Wada, Kitamura, T., Kambe, S., Murasawa, S., Mori, H., et al. (2001). Hydrothermal synthesis of nanosized anatase and rutile TiO2 using amorphous phase TiO2. *Journal of Materials Chemistry, 11,* 1694–1703.

Yuan, N. Y., Tsai, R. Y., Ho, M. H., Wang, D. M., Lai, J. Y., & Hsieh, H. J. (2008). Fabrication and characterization of chondroitin sulfate-modified chitosan membranes for biomedical applications. *Desalination, 234,* 166–174.

Zawadzki, J., & Kaczmarek, H. (2010). Thermal treatment of chitosan in various conditions. *Carbohydrate Polymers, 80,* 394–400.

Zhang, X. Y., Li, H. P., Cui, X. L., & Lin, Y. (2010). Graphene/TiO_2 nanocomposites: Synthesis, characterization and application in hydrogen evolution from water photocatalytic splitting. *Journal of Materials Chemistry, 20,* 2801–2806.

Zhang, X., Sun, Y., Cui, X., & Jiang, Z. (2012). A green and facile synthesis of TiO_2/graphene nanocomposites and their photocatalytic activity for hydrogen evolution. *International Journal of Hydrogen Energy, 37,* 811–815.

Zhao, L., Chang, J., & Zhai, W. (2009). Preparation and HL-7702 cell functionality of titania/chitosan composite scaffolds'. *Journal of Materials Science Materials in Medicine, 20,* 949–957.

The Importance of Nano-materials Characterization Techniques

Yazan Al Thaher, Balakumar Chandrasekaran and Sarojini Jeeva Panchu

Abstract The potential application of nanotechnology in the medical field ranges from nanomaterials and biological devices, to nanoelectronics biosensors, can be extended to molecular nanotechnology like biological machines. Nanomaterial characterization is a keystone for the development and adoption of nanomaterials for certain applications. The unique and novel physico-chemical properties of nanomaterial gave rise to a number of characterization techniques. Therefore, nanoparticles are characterized to study various physical and chemical features such as composition, structure size, morphology, surface area, optical properties, surface composition, oxidation state, and electrochemistry. The characterization of nanomaterials should not be limited to a single technique, because usually multiple measurements are needed to capture all pertinent nanomaterial characteristics. Hence, in this chapter, details of different characterization techniques such as transmission electron microscopy (TEM), atomic force microscopy (AFM), scanning electron microscopy (SEM), X-ray diffraction (XRD), dynamic light scattering (DLS), infrared spectroscopy (IR), and zeta potential (ZP) are discussed.

Keywords Nanomaterials · X-ray diffraction · Transmission electron microscopy · Dynamic light scattering · Zeta potential · Scanning electron microscopy

1 Introduction

Nanomedicine utilizes nanomaterials for the diagnosis, prevention and therapy of various diseases, which has witnessed increasing research interest in recent years. Nanomaterial is defined as the particles having a size between 1 and 100 nm, or at least having one dimension in the range of sub-nanometer to 10 nm (Petros and DeSimone 2010; Duncan and Gaspar 2011). Research on nanomaterials has been conducted in

Y. Al Thaher · B. Chandrasekaran (✉)
Faculty of Pharmacy, Philadelphia University, P. O. Box 1, 19392 Amman, Jordan
e-mail: balakumar@philadelphia.edu.jo

S. J. Panchu
Department of Physics, School of Chemistry and Physics, University of KwaZulu-Natal, Westville, P. O. Box 4000, Durban, South Africa

A. Krishnan and A. Chuturgoon (eds.), *Integrative Nanomedicine for New Therapies*, Engineering Materials,
https://doi.org/10.1007/978-3-030-36260-7_2